Journal of Materials Chemistry C

ROYAL SOCIETY OF CHEMISTRY

PAPER

View Article Online
View Journal | View Issue

Cite this: J. Mater. Chem. C, 2022, 10, 4947

Harnessing near-infrared light *via* S_0 to T_1 sensitizer excitation in a molecular photon upconversion solar cell†

Drake Beery, ‡ Ashley Arcidiacono,‡ Jonathan P. Wheeler, Jiaqi Chen and Kenneth Hanson *

Integrating molecular photon upconversion *via* triplet–triplet annihilation (TTA-UC) directly into a solar cell offers a means of harnessing sub-bandgap, near infrared (NIR) photons and surpassing the Shockley–Queisser limit. However, all integrated TTA-UC solar cells to date only harness visible light. Here, we incorporate an osmium polypyridal complex (Os) as the triplet sensitizer in a metal ion linked multilayer photoanode that is capable of harnessing NIR light *via* S_0 to T_1* excitation, triple energy transfer to a phosphonated bis(9,10-diphenylethynyl)anthracene annihilator (A), TTA-UC, and electron injection into TiO_2 from the upcoverted state. The TiO_2-A-Zn-Os devices have five-fold higher photocurrent ($\sim$3.5 μA cm^{-2}) than the sum of their parts. IPCE data and excitation intensity dependent measurements indicate that the NIR photons are harvested through a TTA-UC mechanism. Transient absorption spectroscopy is used to show that the low photocurrent, as compared to visible light harnessing TTA-UC solar cells, can be atributed to: (1) slow sensitizer to annihilator triplet energy transfer, (2) a low injection yield for the annihilator, and (3) fast back energy transfer from the upconverted state to the sensitizer. Regardless, these results serve as a proof-of-concept that NIR photons can be harnessed *via* an S_0 to T_1* sensitizer excited, integrated TTA-UC solar cell and that further improvements can readily be made by remedying the performance limiting processes noted above.

Received 1st November 2021,
Accepted 24th February 2022

DOI: 10.1039/d1tc05270e

rsc.li/materials-c

Introduction

Solar energy conversion is a critical approach for meeting ever growing energy demands and mitigating the effects of anthropomorphic climate change. Consequently, there is a continuing push to reduce costs and increase solar cell efficiencies. Accounting for the optimum balance between thermalization, transmission, and other losses, the maximum theoretical efficiency for a single-junction solar cell is $\sim$33% (a.k.a., the Shockley–Queisser limit).[1] A promising strategy to surpass this limit is to harness the transmitted, low energy photons using photon upconversion *via* triplet–triplet annihilation (TTA-UC).[2] TTA-UC combines two, low energy photons to generate one higher energy excited state and can be achieved even under low intensity, non-coherent irradiation.[3] Theoretical analyses indicate that if harnessed in a solar cell TTA-UC could increase the maximum efficiency limit to $>$43%.[4]

TTA-UC can be harnessed in a solar cell using either optically[5–9] or electronically coupled schemes.[10–17] The latter relies on incorporating sensitizer and annihilator molecules directly into the solar cell and has achieved photocurrent enhancements up to 0.315 mA cm^{-2}.[18] While a promising proof of concept, all electronically coupled TTA-UC solar cells to date absorb visible light (*i.e.*, $<$700 nm). To maximize the utility of TTA-UC, it is necessary to upconvert and harness near infrared (NIR) photons (*i.e.*, $>$700 nm).[4] It has been estimated that upconverting photons from 800–1000 nm and harnessing them at a 20% photon to current efficiency could increase the short circuit current (J_{sc}) and power conversion efficiencies (PCE) of record solar cells by $\sim$2.5 mA and $\sim$2 percentage points, respectively.[19]

Near infrared to visible TTA-UC requires the appropriate annihilator and sensitizer pair with the latter absorbing at $>$700 nm.[20–22] Molecules that exhibit direct S_0 to T_1* excitation are particularly intriguing as sensitizers because they not only exhibit low energy absorption but also circumvent energy losses associated with intersystem crossing from S_1* to T_1*.[20] Although a spin forbidden process, S_0 to T_1* absorption is common in osmium(II) containing polypyridyl complexes which

Department of Chemistry & Biochemistry, Florida State University, Tallahassee, Florida 32306, USA. E-mail: hanson@chem.fsu.edu

† Electronic supplementary information (ESI) available. See DOI: 10.1039/d1tc05270e

‡ These authors contributed equally to the work.

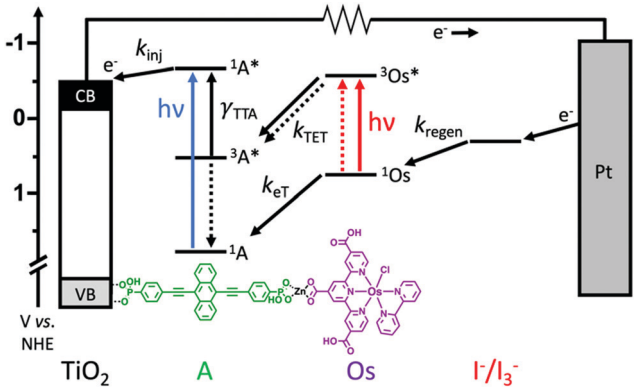

Fig. 1 Integrated TTA-UC solar cell architecture with energetics and dynamics as well as the structure of A and Os. (k_{inj} = electron injection, γ_{TTA} = second order rate constant for TTA, k_{TET} = triplet energy transfer, k_{eT} = electron transfer, and k_{regen} = regeneration rate constants).

has been applied as a sensitizer in both dye-sensitized solar cells (DSSCs),[23,24] and TTA-UC.[25–27] One fundamental limitation with these sensitizers is that the same heavy atom effect that enables the S_0 to T_1* transition also results in a relatively short triplet excited state lifetime, typically <10 ns, that hinders diffusion limited triplet energy transfer necessary for TTA-UC.

Here we incorporate NIR absorbing Os(II) complexes into metal oxide bound, metal ion linked molecular multilayers[28–30] with the goal of overcoming diffusion limited triplet energy transfer dynamics and generating an integrated TTA-UC solar cell. The device architecture and energetics are depicted in Fig. 1. The photoanode is composed of mesoporous TiO_2, a phosphonated annihilator molecule (**A**), a zinc linking ion, and carboxylated osimum(II) polypyridyl sensitizers (**Os**). As shown in Fig. 1, the proposed mechanism is S_0 to T_1* absorption by **Os**, ^{3}**Os*** to **A** triplet energy transfer (k_{TET}), TTA, and electron injection from ^{1}**A*** (k_{inj}). Herein we show that device measurements support a TTA-UC photocurrent generation mechanism, but the performance (~3.5 μA cm^{-2}) is lower than previous integrated TTA-UC solar cells. Using time-resolved spectroscopy we demonstrate that the low performance can be attributed to a combination of slow TET and low electron injection yield due to competitive back energy transfer from ^{1}**A*** to **Os**.

Experimental section

Materials and methods

Zinc acetate dihydrate (Alfa Aesar), 1-butyl-3-methylimidazolium (Sigma-Aldrich), iodine (Sigma-Aldrich), 4-tert-butylpyridine (Sigma-Aldrich), H_2PtCl_6 (Alfa Aesar), and polyethylene glycol bisphenol A epichlorohydrin copolymer (Sigma-Aldrich) were purchased from their respective suppliers, in parenthesis, and used as received. ((anthracene-9,10-diylbis(ethyne-2,1-diyl))bis(4,1-phenylene))bis(phosphonic acid) (**A**), [Os(H$_3$tcterpy)(bpy)Cl]PF$_6$ (**Os**),[23] triphenyl-4,4′-diphosphonic acid (**B**),[31] and TiO_2/ZrO_2 sol-gels[32] were synthesized according to previous procedures with any modifications described in the ESI.† All other reagents and solvents (analytical reagent grade) were purchased and used without further purification from Sigma-Aldrich. Fluorine-doped tin oxide (FTO) coated glass (sheet resistance 15 Ω □$^{-1}$) was purchased from Hartford Glass Co. Meltonix film (1170-25) and Vac'n Fill Syringe (65209) were purchased from Solaronix. Micro glass cover slides (18 × 18 mm) were obtained from VWR.

Device assembly

TiO_2 films were cast using the doctor blade method (3 M Scotch^{TM} tape) onto a FTO-glass substrate then sintered in an oven at 500 °C for 15 min.[10] The resulting films were then immersed into a 1 mM or 200 μM solution of **A** or **B**, respectively in DMSO for 48 hours then rinsed with methanol and dried under a stream of air. Next, the films were immersed into a 0.5 μM solution of Zn(CH$_3$COO)$_2$ in MeOH for 3 hours then rinsed with MeOH and dried. Following this, the films were immersed in a 1 mM solution of **Os** in a 1 : 1 mixture of *tert*-butanol and MeCN for 24 hours[23] then rinsed with MeOH and dried. The resulting films were etched to a 1 × 1 cm active area and used as the anode. The Pt cathode was prepared by drop-casting H_2PtCl_6 solution in ethanol (50 μL, 5 mM) that was heat-dried at 400 °C for 20 min. The films were then sealed together using Melatonix thermoplastic at 150 °C using a home built pressure and heating apparatus.[33] The sandwiched cells were then transferred to a glovebox where dry and oxygen free MeCN containing 0.1 M BMII/0.01 M I_2/0.1 M TBP was injected using a Vac'n Fill Syringe (Solaronix) and solvent injection hole was sealed using thermoplastic and a small glass cover slip heated with a soldering iron.

Characterization

Instrumentation. UV-Vis absorption, NMR, MS, ATR-FTIR, incident photon to current efficiency (IPCE), amperometric current–time (*i*–*t*), intensity dependence, steady-state and time-resolved emission, and transient absorption measurements were performed on previously described instrumentation and details are provided in the ESI.†[,13,34]

Surface coverages. Surface coverages (Γ in nmol cm^{-2}) were estimated with the expression $\Gamma = (A(\lambda_{abs})/\varepsilon(\lambda))/1000$,[35] where $A(\lambda)$ is the absorbance of each component on the fully loaded films and ε is the molar extinction coefficient of A (ε_{440nm} = 9.4 × 10^3 M^{-1} cm^{-1}) and Os (ε_{888nm} = 3.1 × 10^3 M^{-1} cm^{-1})[25] in DMSO.

Results & discussion

Multilayer assembly

The photoanode in these devices is composed of nanocrystalline TiO_2, ((anthracene-9,10-diylbis(ethyne-2,1-diyl))bis(4,1-phenylene))bis(phosphonic acid) (**A**), Zn^{2+} linking ions, and [Os(H$_3$tcterpy)(bpy)Cl]PF$_6$ (**Os**) as depicted in Fig. 1. **A** was chosen as the annihilator molecule because the parent 9,10-bis(phenylethynyl)anthracene,[10,36] is known to facilitate TTA and also has sufficient potential for electron injection into the conduction band of TiO_2 (−0.5 V *vs.* NHE)[37] from the singlet

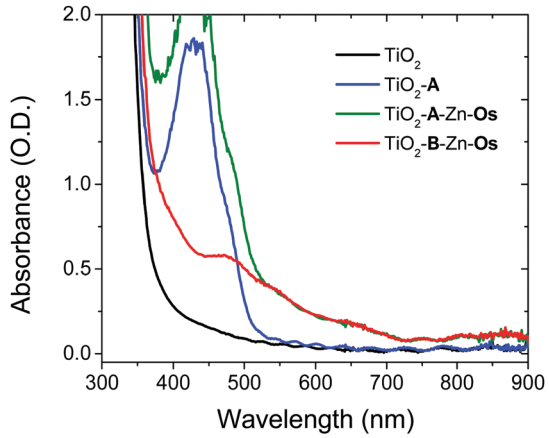

Fig. 2 Absorption spectra of dry TiO_2, TiO_2-**A**, TiO_2-**B**-Zn-**Os**, and TiO_2-**A**-Zn-**Os** films.

(^{1}**A***/**A**$^+$ = −0.64 V) but not triplet (^{3}**A***/**A**$^+$ = −0.15 V) excited state.[10] Phosphonate binding groups were chosen for **A** because they exhibit greater surface stability than COOH,[38] and will prevent competitive desorption during subsequent loading steps. **A** was synthesized in five steps using slight variations of known procedures[38–41] with details provided in the ESI.†

Os was selected as the sensitizer because it is a known NIR absorbing dye, it has COOH binding groups, and has been used as the triplet sensitizer for TTA-UC.[23,25] Additionally, the triplet excited state energy of **Os** (~1.3 eV) is sufficient for favourable triplet energy transfer to **A** (1.2 eV).[36]

The films were prepared by a stepwise soaking procedure and monitored with UV-Vis (Fig. 2) and ATR-IR (Fig. S4, ESI†) spectroscopy. First, the ~4 μm thick nanocrystalline TiO_2 film was submerged in a 1 mM solution of **A** in DMSO for 48 h, followed by a 0.5 μM solution of $Zn(OAc)_2$ in MeOH for 3 h, and finally a 1 mM solution of **Os** in a 1 : 1 mixture of *tert*-butanol and acetonitrile. As can be seen in Fig. 2, the absorption spectrum of the bilayer film is the summed contribution of each chromophore. From spectral deconvolution, surface coverages of 175 nmol cm^{-2} and 25 nmol cm^{-2} were determined for **A** and **Os**, respectively, giving an ~7 : 1 annihilator to sensitizer ratio (see the ESI† for details). In the absence of Zn^{2+} treatment, no **Os** loading was observed on TiO_2-**A** (Fig. S6, ESI†) indicating that the above procedure results in a multilayer structure (TiO_2-**A**-Zn-**Os**) and not simply a co-deposited film.

The films were incorporated into a standard sandwich DSSC architecture with TiO_2-dye as the photoanode, Pt coated FTO glass as the cathode, and I^-/I_3^- as the redox mediator (0.1 M BMII/0.01 M I_2/0.1 M TBP in acetonitrile). For comparative purposes, a series of devices were prepared with photoanodes composed of anthracene only (TiO_2-**A**), the **A**-Zn-**Os** bilayer (TiO_2-**A**-Zn-**Os**) and a sensitizer only bilayer (TiO_2-**B**-Zn-**Os**). For the latter device, the photophysical and electrochemically inert triphenyl-4,4′-diphosphonic acid bridging molecule (**B**) was used as a means of mimicking the spatial separation between **Os** and TiO_2 in the bilayer but without concerns of light absorption or energy/electron transfer to **B**.[34]

Photovoltaic characterization

The short circuit photocurrent density (J_{sc}) was measured under solar irradiance (AM1.5) and the results are shown in Fig. 3a. A 570 nm long pass filter was used to selectively excite the **Os** sensitizer and avoid direct excitation and electron injection from **A**. Under these conditions, less than 0.5 μA cm^{-2} photocurrent was observed from TiO_2-**A** and TiO_2-**B**-Zn-**Os**. In contrast, the TiO_2-**A**-Zn-**Os** device generated a ~3.5 μA cm^{-2} photocurrent which is an ~5 fold increase in photocurrent compared to the sum of the individual components.

The incident photon-to-current efficiency spectra (IPCE) of TiO_2-**A**-Zn-**Os** (Fig. 3b) resembles its absorptance spectra with a

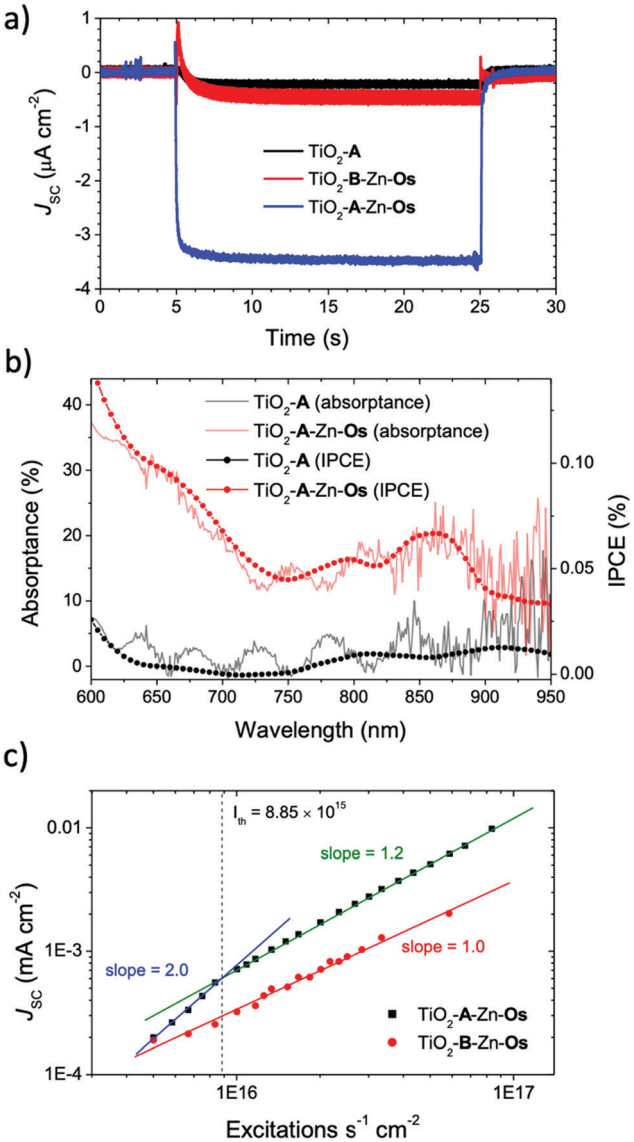

Fig. 3 (a) Amperometric *i*–*t* curves under 1 equivalent AM 1.5 solar irradiation passed through a 570 nm long pass filter (shutter open at *t* = 5 s, shutter closed at *t* = 25 s), (b) IPCE and absorptance spectra for TiO_2-**A**-Zn-**Os** and TiO_2-**A**, and (c) J_{sc} with respect to excitation rate for TiO_2-**A**-Zn-**Os** and TiO_2-**B**-Zn-**Os** (λ_{ex} = 635 nm). All measurements were obtained at 0 V.

broad low energy peak at ~850 nm and photocurrent contribution out to at least 950 nm (*i.e.*, the limit of our broad band light source). In contrast, nominal current was observed from TiO_2-**A** and TiO_2-**B**-Zn-**Os** further indicating that direct excitation and electron injection from **Os** is not a major contributor to the photocurrent. Consequently, IPCE measurements indicate that TiO_2-**A**-Zn-**Os** enables the harnessing of NIR light *via* a cooperative photon to current generation process.

Further insights into the photocurrent generation mechanism by TiO_2-**B**-Zn-**Os** and TiO_2-**A**-Zn-**Os** were obtained with excitation intensity *versus* photocurrent density measurements. As can be seen in Fig. 3c, the sensitizer only control device (TiO_2-**B**-Zn-**Os**) exhibited a linear response (slope = 1.0) throughout the entire intensity range which is consistent with direct excitation and electron injection from **Os*** into TiO_2. In contrast, the TiO_2-**A**-Zn-**Os** device exhibits a quadratic (slope = 2.0) to linear (slope ≈ 1.0) dependence when transitioning from low to high intensity excitation. This quadratic-to-linear behavior is consistent with a TTA-UC photocurrent generation mechanism.[42,43]

The intensity threshold between the quadratic and linear regimes, or I_{th} value, is the minimum excitation intensity necessary for TTA-UC to reach its maximum efficiency.[43,44] For the TiO_2-**A**-Zn-**Os** device under 635 nm excitation, the I_{th} value is 8.7 mW cm^{-2} (Fig. S11, ESI†) or in terms of excitations per second (*i.e.*, photons s^{-1} cm^{-2} × absorptance) 8.85 × 10^{15} s^{-1} cm^{-2}. To provide context, the integrated AM1.5 solar intensity from 570–1000 nm is 44.8 mW cm^{-2} or ~10 mW cm^{-2} assuming an absorptance of 20%.

Collectively the above results indicate that in addition to the visible spectrum, the TiO_2-**A**-Zn-**Os** device is harnessing nearIR light out to 900 nm and doing so through a TTA-UC photocurrent generation mechanism. However, the ~3.5 μA cm^{-2} photocurrent is at least an order of magnitude lower than that obtained in the visible region.[18] It is worth acknowledging that there is an approximately 50% decrease in solar intensity from 500 to 1000 nm but that alone cannot account for the decrease in performance.

Energy and electron transfer dynamics

To gain insights into the rate and efficiency limiting processes in the TiO_2-**A**-Zn-**Os** device we monitored event dynamics using transient absorption spectroscopy (TA). The results are shown in Fig. 5–7 with additional spectra provided in the ESI.† Due to experimental limitations, the excitation intensities for TA measurements (7 mJ cm^{-2} at 475 nm and 15 mJ cm^{-2} at 650 nm) are much higher than solar flux and thus are conducted in the linear TTA-UC regime. However, it has been previously shown that interlayer energy transfer and electron injection dynamics quantified below are largely independent of the number of excitation events.[34] Biexcitonic processes like TTA are fluence dependent but were not monitored here.

The productive and non-productive events of interest are depicted in Fig. 4 in green and red, respectively, and the species involved in each process are summarized in eqn (1)–(6).

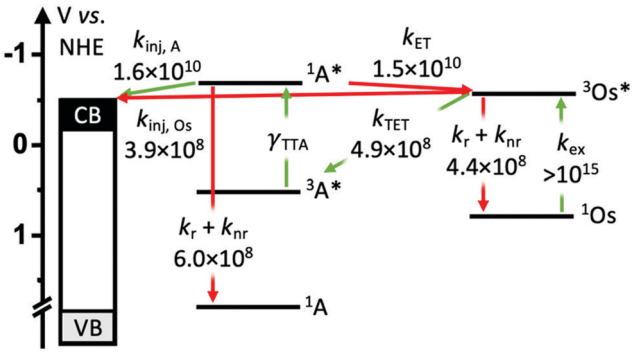

Fig. 4 Productive (green) and non-productive (red) dynamic events that occur in the TiO_2-**A**-Zn-**Os** bilayer with their associated experimentally determined rate constants (all units in s^{-1}). (k_{inj} = electron injection, k_r = radiative decay, k_{nr} = non-radiative decay, k_{TET} = triplet energy transfer, k_{ET} = back energy transfer, k_{ex} = excitation).

$$k_{nr+r(Os)}: {}^3Os^* \rightarrow {}^1Os \quad (1)$$

$$k_{TET}: {}^3Os^* + {}^1A \rightarrow {}^1Os + {}^3A^* \quad (2)$$

$$k_{inj(Os)}: TiO_2\text{-B-Zn-}{}^3Os^* \rightarrow TiO_2(e^-)\text{-B-Zn-}Os^+ \quad (3)$$

$$k_{nr+r(A)}: {}^1A^* \rightarrow {}^1A \quad (4)$$

$$k_{inj(A)}: TiO_2\text{-}{}^1A^* \rightarrow TiO_2(e^-)\text{-}A^+ \quad (5)$$

$$k_{ET}: {}^1A^* + {}^1Os \rightarrow {}^1A + {}^3Os^* \quad (6)$$

Following excitation, we presume that **^{3}Os*** can decay *via* three primary mechanisms. The first is *via* intrinsic radiative and non-radiative decay ($k_{nr+r(Os)}$; eqn (1)). The transient absorption decay kinetics for **Os** in DMSO solution (*i.e.*, in the absence of any quenching species) could be fit to a single exponential equation giving $1/\tau = k_{nr+r(Os)} = 4.4 \times 10^8$ s^{-1} (Fig. 5).

In the TiO_2-**A**-Zn-**Os** bilayer film **^{3}Os*** can also decay *via* TET (eqn (2)) and electron injection into TiO_2 (eqn (3)). To probe **^{3}Os*** to **A** triplet energy transfer we monitored the excited state decay of **^{3}Os*** at 500 nm in ZrO_2-**A**-Zn-**Os** when only **Os** is

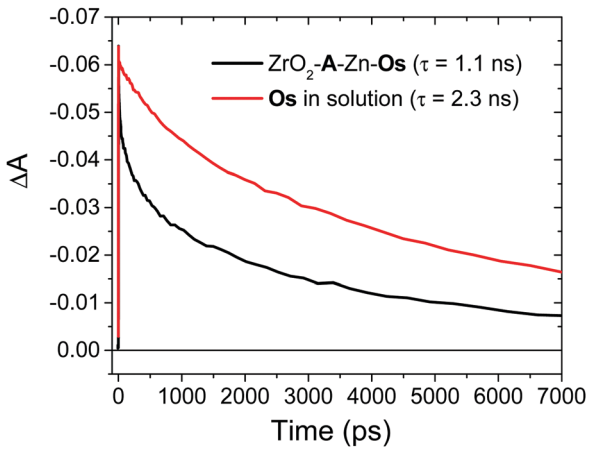

Fig. 5 Transient absorption decay traces at 500 nm for **Os** in DMSO (red) and ZrO_2-**A**-Zn-**Os** in MeCN (black). (λ_{ex} = 650 nm).

excited (λ_{ex} = 650 nm) and the results are shown in Fig. 5. ZrO_2 was selected as the substrate for these measurements because in contrast to TiO_2, its relatively high conduction band (>2.0 V *vs.* NHE)[45] hinders excited state electron transfer to the metal oxide substrate so photophysical events can be quantified in the absence of electron injection (Fig. S12, ESI†). Thus, assuming that the only additional decay channel present in ZrO_2-**A**-Zn-**Os** is TET,[34] then k_{TET} can be calculated using eqn (7):

$$k_{TET} = \frac{1}{\tau_{Os(bl)}} - \frac{1}{\tau_{Os}} \quad (7)$$

where τ_{Os} is the lifetime of **Os** in solution and $\tau_{Os(bl)}$ is the ^{3}**Os***lifetime in the ZrO_2-**A**-Zn-**Os** bilayer. As can be seen in Fig. 5, there is a decrease in excited state lifetime from 2.3 to 1.1 ns in the presence of **A** giving a calculated k_{TET} of 4.9 × 10^8 s^{-1}.

Excited state Osmium(II) polypyridyl complexes are also known to inject electrons into TiO_2,[23] albeit in the presence of Li^+ which is known to lower the conduction band of TiO_2 (Li^+ is not present here).[46] To probe electron injection dynamics ($k_{inj(Os)}$; eqn (3)) we monitored the decay of ^{3}**Os*** in TiO_2-**B**-Zn-**Os** ($\tau_{Os(TiO2)}$) and the results are shown in Fig. S15 (ESI†). Assuming the only additional quenching pathway for ^{3}**Os*** in TiO_2-**B**-Zn-**Os** is electron injection, a $k_{inj(Os)}$ of 3.9 × 10^8 s^{-1} was calculated using eqn (8):

$$k_{inj(Os)} = \frac{1}{\tau_{Os(TiO_2)}} - \frac{1}{\tau_{Os}} \quad (8)$$

This electron injection rate is slower than k_{TET} and $k_{nr+r(Os)}$ giving an estimated injection yield of <25%.[31] Additionally, the intensity dependent results in Fig. 3 suggests direct electron injection from ^{3}**Os*** is not the preferred deactivation pathway. If it was significant, we would observe a slope of <2 in the low intensity regime for TiO_2-**A**-Zn-**Os** and a higher photocurrent for TiO_2-**B**-Zn-**Os**.

In the absence of electron injection, the ^{3}**Os*** to **A** triplet energy transfer efficiency (Φ_{TET}) can be calculated using eqn (9).

$$\Phi_{TET} = \frac{k_{TET}}{k_{TET} + k_{nr+r(Os)}} \quad (9)$$

A Φ_{TET} of ~50% suggests that at least half of the absorbed photon energy is being lost *via* emission (k_r) and/or heat dissipation (k_{nr}) by ^{3}**Os***. Increasing the Φ_{TET} would not only increase the J_{sc} contribution from TTA-UC but also lower the I_{th} value and the maximum efficiency onset.

^{3}**Os*** to **A** TET and then bimolecular TTA between two ^{3}**A*** results in the formation of the upconverted ^{1}**A*** state. In the absence of a quencher (*i.e.*, for **A** in solution) ^{1}**A*** decays *via* radiative and non-radiative pathways ($k_{nr+r(A)}$; eqn (4)) with a lifetime of 1.6 ns and rate constant of 6.0 × 10^8 s^{-1} (Fig. S16, ESI†). The spectra and kinetics for **A** in solution, as opposed to on ZrO_2, were selected for the following analyses because although the time-resolved emission decays for both samples are similar (Fig. S2 and S17, ESI†) the former had a much better signal-to-noise ratio in the TA measurements.

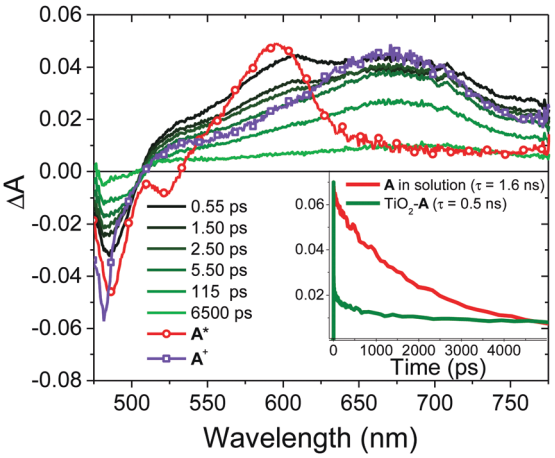

Fig. 6 TA spectral evolution of TiO_2-**A** from black to green with overlays of **A** in solution (red), and a spectrum consistent with $\mathbf{A}^+$ (purple) from the 6.5 ns time slice of TiO_2-**A**. The inset contains decay traces at 605 nm for solution **A** and TiO_2-**A**. (λ_{ex} = 475 nm).

On TiO_2, **A** has sufficient excited state potential for electron injection into the metal oxide substrate ($k_{inj(A)}$; eqn (5)).[10] We probed the electron transfer dynamics for TiO_2-**A** and the results are shown in Fig. 6. TiO_2-**A**, as opposed to TiO_2-**A**-Zn-**Os**, was selected for these measurements to allow for selective excitation and monitoring of **A** without simultaneous excitation of **Os** (Fig. 2). But previous results have shown that metal ion coordination and bilayer formation has minimal impact of the intrinsic photophysical properties of the first layer chromophore.[47]

In the early time slices we see a distinct peak at ~600 nm that is consistent with the excited state absorption from ^{1}**A*** in solution (red spectrum in Fig. 6). That feature rapidly decreases and a broad peak at ~675 nm remains present beyond our ~7 ns acquisition window which we attribute to the formation of the $TiO_2(e^-)$-$\mathbf{A}^+$ charge separated species. $k_{inj(A)}$ can then be calculated using eqn (10):

$$k_{inj(A)} = \frac{1}{\tau_{A(TiO_2)}} - \frac{1}{\tau_A} \quad (10)$$

where τ_A is the lifetime of ^{1}**A*** in solution (1.6 ns) and $\tau_{A(TiO_2)}$ is the lifetime of the ^{1}**A*** feature in TiO_2-**A** (0.46 ns). The calculated $k_{inj(A)}$ of 1.6 × 10^{10} s^{-1} is an order of magnitude slower than our previously reported 4.5 × 10^{11} s^{-1} for 4,4′-(anthracene-9,10-diyl)bis(4,1-phenylene) diphosphonic acid which lacks the acetylene spacer of **A**.[34] Presumably a combination of decreased excited state potential and increased spatial separation between the anthracene core and TiO_2 is responsible for the decrease in electron injection rate. Regardless, the observed photocurrent from TiO_2-**A**-Zn-**Os** indicates that electron transfer is sufficiently fast for at least some charge separation and photocurrent generation.

Back energy transfer from the upconverted singlet state of the annihilator to sensitizer (k_{ET}; eqn (6)) is a well-known, non-productive process in TTA-UC.[19] To probe k_{ET}, we measured the

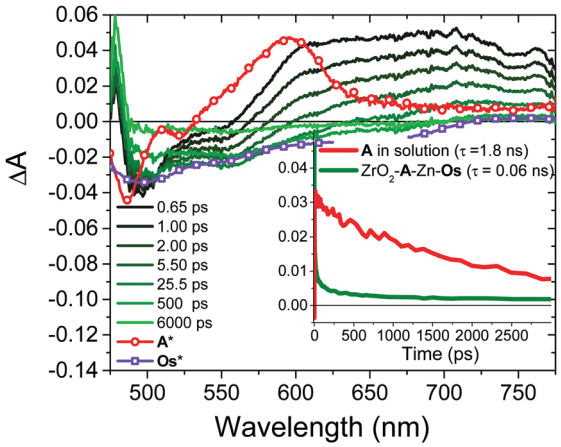

Fig. 7 Spectral evolution from ZrO_2-**A**-Zn-**Os** from black to green following 475 nm excitation with overlays of solution spectra of **A** (red, λ_{ex} = 475 nm) and **Os** (purple, λ_{ex} = 650 nm). The inset contains decay traces at 750 nm for solution **A** and ZrO_2-**A**-Zn-**Os** (λ_{ex} = 475 nm).

excited state dynamics of ZrO_2-**A**-Zn-**Os** following 475 nm excitation and the results are shown in Fig. 7.

Due to the broad absorption of **Os** (Fig. 2), it was not possible to selectively excite **A** so even at the earliest time slices we see a mixed contribution from both ^{3}**Os*** and ^{1}**A*** where the ground state bleach of the former below 600 nm offsets the excited state absorption of the latter in the same region. However, at 750 nm there is minimal contribution of ^{3}**Os*** and thus ^{1}**A*** can be preferentially monitored. A k_{ET} of 1.5 × 10^{10} s^{-1} was calculated using eqn (10):

$$k_{ET} = \frac{1}{\tau_{A(bl)}} - \frac{1}{\tau_A} \quad (11)$$

where $\tau_{A(bl)}$ is the ^{1}**A*** lifetime in the ZrO_2-**A**-Zn-**Os** bilayer. This k_{ET} is orders of magnitude larger than previously observed for diphenyl anthracene-Zn–Pt(II) porphyrin multilayer.[34,47] Presumably any decreases in rate due to increased spatial separation between the anthracene and osmium transition dipole moments[48] are offset by the near unity spectral overlap between emission from **A** and absorption of **Os**. This observation further emphasizes the utility of an absorption gap between the Soret and Q bands of metalloporphyrins and their continued popularity as sensitizers for TTA-UC.[49] It is important to mention that while Fig. 4 depicts a ^{1}**A*** to ^{3}**Os*** energy transfer process, this was done for the sake of simplicity because we have no evidence to support a particular mechanism (*e.g.*, FRET *versus* Dexter) or the spin state generated (*e.g.*, ^{3}**Os*** *versus* ^{1}**Os***).

With the rate constants above, an electron injection yield for ^{1}**A*** into TiO_2 ($\Phi_{inj(A)}$) can be calculated using eqn (12).

$$\Phi_{inj(A)} = \frac{k_{inj(A)}}{k_{inj(A)} + k_{ET} + k_{nr+r(A)}} \quad (12)$$

The ~50% injection yield can be directly attributed to back energy transfer being highly competitive with the electron injection rate. Consequently, at least half of the upconverted states transfer their energy back to **Os** prior to injection. While not an absolute loss pathway since it results in regeneration of ^{3}**Os***, one excited state was consumed during upconversion and the TTA-UC cycle must be re-initiated *via* TET.

Despite favorable driving force (Fig. 4), we saw no evidence of **Os** to $\mathbf{A}^+$ electron transfer occurring in the TiO_2-**A**-Zn-**Os** film. While interlayer electron transfer has been observed,[50] the increased distance and geometric constraint imparted by the metal ion linkage can also hinder electron transfer.[48] Consequently, the post injection cation resides on **A** and is likely the site of regeneration where access by the mediator is still possible due to the lower surface coverage of **Os** relative to **A** (~7 : 1).[15]

Conclusions

In this study, we have incorporated an Osmium polypyridyl complex as the senstitizer in a metal ion linked multilayer on TiO_2 for application as the photoanode in an integrated TTA-UC solar cell. Photocurrent, IPCE, and intensity dependent measurements indicate that direct S_0 to T_1* excitation of the osmium complex can be used to harness NIR light and generate photocurrent *via* TTA-UC. Although, the ~3.5 μA cm^{-2} photocurrent contribution from TTA-UC is at least an order of magnitude lower than those typically obtained in the visible region. Based on transient absorption measurements the low performance can be attributed to: (1) slow sensitizer to annihilator triplet energy transfer, (2) a low injection yield for the annihilator, and (3) fast back energy transfer from the upconverted state to the sensitizer. Nonetheless, this work demonstrates that NIR, S_0 to T_1* excitation can be harnessed in an integrated TTA-UC solar cell (J_{sc} ≈ 3.5 μA cm^{-2}) with a five-fold increase in photocurrent compared to the sum of its parts, but this is still well below device relevant photocurrent contributions (>100 μA cm^{-2}).[2] Further improvements can be readily achieved using (1) sensitizers with increased triplet excited state lifetimes, (2) an annihilator with increased driving force and decreased spatial separation between the chromophoric unit and the TiO_2 surface for increased electron injection yields, and (3) a balance of driving force and distance between the sensitizer and annihilator molecule for maximized triplet energy transfer and minimized back, singlet energy transfer.

Conflicts of interest

There are no conflicts to declare.

Acknowledgements

This work was supported by the National Science Foundation under Grant No. DMR-1752782. Ultrafast transient absorption measurements were performed on a spectrometer supported by the National Science Foundation under Grant No. CHE-1919633. A portion of these measurements were conducted in the FSU Department of Chemistry & Biochemistry's Mass Spec

(FSU075000-MASS), NMR (FSU075000NMR), and Materials Characterization (FSU075000MAC) Laboratories.

Notes and references

1 W. Shockley and H. J. Queisser, *J. Appl. Phys.*, 1961, **32**(3), 510–519.
2 D. Beery, T. W. Schmidt and K. Hanson, *ACS Appl. Mater. Interfaces*, 2021, **13**(28), 32601–32605.
3 T. N. C. Singh-Rachford and N. Felix, *Coord. Chem. Rev.*, 2010, **254**(21–22), 2560–2573.
4 N. J. Ekins-Daukes and T. W. Schmidt, *Appl. Phys. Lett.*, 2008, **93**(6), 063507.
5 Y. Y. Cheng, B. Fückel, R. W. MacQueen, T. Khoury, R. G. C. R. Clady, T. F. Schulze, N. J. Ekins-Daukes, M. J. Crossley, B. Stannowski, K. Lips and T. W. Schmidt, *Energy Environ. Sci.*, 2012, **5**(5), 6953–6959.
6 T. F. Schulze, Y. Y. Cheng, B. Fückel, R. W. MacQueen, A. Danos, N. J. L. K. Davis, M. J. Y. Tayebjee, T. Khoury, R. G. C. R. Clady, N. J. Ekins-Daukes, M. J. Crossley, B. Stannowski, K. Lips and T. W. Schmidt, *Aust. J. Chem.*, 2012, **65**(5), 480–485.
7 T. F. Schulze, J. Czolk, Y.-Y. Cheng, B. Fückel, R. W. MacQueen, T. Khoury, M. J. Crossley, B. Stannowski, K. Lips, U. Lemmer, A. Colsmann and T. W. Schmidt, *J. Phys. Chem. C*, 2012, **116**(43), 22794–22801.
8 Y. Y. Cheng, A. Nattestad, T. F. Schulze, R. W. MacQueen, B. Fückel, K. Lips, G. G. Wallace, T. Khoury, M. J. Crossley and T. W. Schmidt, *Chem. Sci.*, 2016, **7**(1), 559–568.
9 A. Monguzzi, S. M. Borisov, J. Pedrini, I. Klimant, M. Salvalaggio, P. Biagini, F. Melchiorre, C. Lelii and F. Meinardi, *Adv. Funct. Mater.*, 2015, **25**(35), 5617–5624.
10 C. Simpson, T. M. Clarke, R. W. MacQueen, Y. Y. Cheng, A. J. Trevitt, A. J. Mozer, P. Wagner, T. W. Schmidt and A. Nattestad, *Phys. Chem. Chem. Phys.*, 2015, **17**(38), 24826–24830.
11 T. Morifuji, Y. Takekuma and M. Nagata, *ACS Omega*, 2019, **4**(6), 11271–11275.
12 S. Ahmad, J. Liu, C. Gong, J. Zhao and L. Sun, *ACS Appl. Energy Mater.*, 2018, **1**(2), 249–253.
13 S. P. Hill, T. Dilbeck, E. Baduell and K. Hanson, *ACS Energy Lett.*, 2016, **1**(1), 3–8.
14 T. Dilbeck, S. P. Hill and K. Hanson, *J. Mater. Chem. A*, 2017, **5**(23), 11652–11660.
15 S. P. Hill and K. Hanson, *J. Am. Chem. Soc.*, 2017, **139**(32), 10988–10991.
16 D. Beery, J. P. Wheeler, A. Arcidiacono and K. Hanson, *ACS Appl. Energy Mater.*, 2020, **3**(1), 29–37.
17 Y. L. Lin, M. Koch, A. N. Brigeman, D. M. E. Freeman, L. Zhao, H. Bronstein, N. C. Giebink, G. D. Scholes and B. P. Rand, *Energy Environ. Sci.*, 2017, **10**(6), 1465–1475.
18 Y. Zhou, C. Ruchlin, A. J. Robb and K. Hanson, *ACS Energy Lett.*, 2019, **4**(6), 1458–1463.
19 T. Dilbeck and K. Hanson, *J. Phys. Chem. Lett.*, 2018, **9**(19), 5810–5821.
20 P. Bharmoria, H. Bildirir and K. Moth-Poulsen, *Chem. Soc. Rev.*, 2020, **49**(18), 6529–6554.
21 L. Nienhaus, M. Wu, N. Geva, J. J. Shepherd, M. W. B. Wilson, V. Bulovi, T. Van Voorhis, M. A. Baldo and M. G. Bawendi, *ACS Nano*, 2017, **11**(8), 7848–7857.
22 E. M. Gholizadeh, S. K. K. Prasad, Z. L. Teh, T. Ishwara, S. Norman, A. J. Petty, J. H. Cole, S. Cheong, R. D. Tilley, J. E. Anthony, S. Huang and T. W. Schmidt, *Nat. Photonics*, 2020, **14**(9), 585–590.
23 S. Altobello, R. Argazzi, S. Caramori, C. Contado, S. Da Fré, P. Rubino, C. Choné, G. Larramona and C. A. Bignozzi, *J. Am. Chem. Soc.*, 2005, **127**(44), 15342–15343.
24 T. Swetha, K. R. Reddy and S. P. Singh, *Chem. Rec.*, 2015, **15**(2), 457–474.
25 S. Amemori, Y. Sasaki, N. Yanai and N. Kimizuka, *J. Am. Chem. Soc.*, 2016, **138**(28), 8702–8705.
26 R. Haruki, Y. Sasaki, K. Masutani, N. Yanai and N. Kimizuka, *Chem. Commun.*, 2020, **56**(51), 7017–7020.
27 Y. Sasaki, M. Oshikawa, P. Bharmoria, H. Kouno, A. Hayashi-Takagi, M. Sato, I. Ajioka, N. Yanai and N. Kimizuka, *Angew. Chem., Int. Ed.*, 2019, **58**(49), 17827–17833.
28 A. J. Robb, E. S. Knorr, N. Watson and K. Hanson, *J. Photochem. Photobiol., A*, 2020, **390**, 112291.
29 J. C. Wang, S. P. Hill, T. Dilbeck, O. O. Ogunsolu, T. Banerjee and K. Hanson, *Chem. Soc. Rev.*, 2018, **47**(1), 104–148.
30 K. Hanson, D. A. Torelli, A. K. Vannucci, M. K. Brennaman, H. Luo, L. Alibabaei, W. Song, D. L. Ashford, M. R. Norris, C. R. K. Glasson, J. J. Concepcion and T. J. Meyer, *Angew. Chem., Int. Ed.*, 2012, **51**(51), 12782–12785.
31 J. C. Wang, I. A. Murphy and K. Hanson, *J. Phys. Chem. C*, 2015, **119**(7), 3502–3508.
32 S.-H. A. Lee, N. M. Abrams, P. G. Hoertz, G. D. Barber, L. I. Halaoui and T. E. Mallouk, *J. Phys. Chem. B*, 2008, **112**(46), 14415–14421.
33 O. O. Ogunsolu, J. C. Wang and K. Hanson, *ACS Appl. Mater. Interfaces*, 2015, **7**(50), 27730–27734.
34 T. Dilbeck, J. C. Wang, Y. Zhou, A. Olsson, M. Sykora and K. Hanson, *J. Phys. Chem. C*, 2017, **121**(36), 19690–19698.
35 L. A. Gallagher, S. A. Serron, X. Wen, B. J. Hornstein, D. M. Dattelbaum, J. R. Schoonover and T. J. Meyer, *Inorg. Chem.*, 2005, **44**(6), 2089–2097.
36 Y. J. Bae, G. Kang, C. D. Malliakas, J. N. Nelson, J. Zhou, R. M. Young, Y.-L. Wu, R. P. Van Duyne, G. C. Schatz and M. R. Wasielewski, *J. Am. Chem. Soc.*, 2018, **140**(45), 15140–15144.
37 A. J. Robb, D. Miles, S. R. Salpage, N. Watson, Q. He, Q. Wu and K. Hanson, *ACS Appl. Mater. Interfaces*, 2020, **12**(34), 38003–38011.
38 K. Hanson, M. K. Brennaman, H. Luo, C. R. K. Glasson, J. J. Concepcion, W. Song and T. J. Meyer, *ACS Appl. Mater. Interfaces*, 2012, **4**(3), 1462–1469.
39 H. Onouchi, K. Maeda and E. Yashima, *J. Am. Chem. Soc.*, 2001, **123**(30), 7441–7442.
40 F. Yu, Y.-M. Zhang, Y.-H. Guo, A.-H. Li, G.-X. Yu and B. Li, *CrystEngComm*, 2013, **15**(41), 8273–8279.

41 S. P. Hill, T. Banerjee, T. Dilbeck and K. Hanson, *J. Phys. Chem. Lett.*, 2015, **6**(22), 4510–4517.
42 A. Haefele, J. Blumhoff, R. S. Khnayzer and F. N. Castellano, *J. Phys. Chem. Lett.*, 2012, **3**(3), 299–303.
43 A. Monguzzi, J. Mezyk, F. Scotognella, R. Tubino and F. Meinardi, *Phys. Rev. B: Condens. Matter Mater. Phys.*, 2008, **78**(19), 195112.
44 Y. Murakami and K. Kamada, *Phys. Chem. Chem. Phys.*, 2021, **23**(34), 18268–18282.
45 R. Katoh, A. Furube, T. Yoshihara, K. Hara, G. Fujihashi, S. Takano, S. Murata, H. Arakawa and M. Tachiya, *J. Phys. Chem. B*, 2004, **108**(15), 4818–4822.
46 C. A. Kelly, F. Farzad, D. W. Thompson, J. M. Stipkala and G. J. Meyer, *Langmuir*, 1999, **15**(20), 7047–7054.
47 A. Arcidiacono, Y. Zhou, W. Zhang, J. O. Ellison, S. Ayad, E. S. Knorr, A. N. Peters, L. Zheng, W. Yang, S. S. Saavedra and K. Hanson, *J. Phys. Chem. C*, 2020, **124**(43), 23597–23610.
48 A. Arcidiacono, A. Robb, R. Masitas, S. Salpage, G. M. McLeod, O. Ogunsolu, J. Chen, M. G. Roper and K. Hanson, *Photochem. Photobiol.*, 2022, **9**, 100088.
49 V. Gray, K. Moth-Poulsen, B. Albinsson and M. Abrahamsson, *Coord. Chem. Rev.*, 2018, **362**, 54–71.
50 O. O. Ogunsolu, I. A. Murphy, J. C. Wang, A. Das and K. Hanson, *ACS Appl. Mater. Interfaces*, 2016, **8**(42), 28633–28640.